

Evidence for increasing dark energy in the Late Universe

Maryam Aghaei Abchouyeh¹ and Maurice H.P.M. van Putten^{1,2,★}

¹ Department of Physics and Astronomy, Sejong University, 98 Gunja-Dong, Gwangjin-gu, Seoul 143-747, Republic of Korea

² INAF-OAS Bologna, via P. Gobetti, 101, I-40129 Bologna Italy

e-mail: maryam@sejong.ac.kr

e-mail: mvp@sejong.ac.kr

Received September 30, 20XX

ABSTRACT

Context. A comprehensive survey of *Baryon Acoustic Oscillation* (BAO) in the *Large Scale Structure* (LSS), in stratified data covering a finite redshift range is provided by the *Dark Energy Spectroscopic Instrument* (DESI). Extracting cosmological parameters in a joint analysis of LSS-CMB data is hereby inherently a nonlinear problem.

Aims. In particular, this nonlinearity may concern the unknown equation of state of dark energy $w(a)$, defined in the general $w(a)$ CDM framework. Nevertheless, a common approach is the linearized approximation hereto notably w_0w_a CDM, also applied by DESI. Here, we consider a potential source of a systematic uncertainty in this linearization due to non-commutativity between w_0w_a CDM and *a posteriori* linearization of $w(a)$ CDM, identified with an intrinsic symmetry in the latter, which is violated in the former. We shall refer to these as early and late linearization, respectively.

Methods. Observational consequences of symmetry violation is inherent to early linearization regardless of choice of data, here elucidated in the analysis of the Hubble expansion in the Local Distance Ladder (LDL) using cosmic chronometer data.

Results. Strikingly, opposite results are found for the evolution of dark energy by early versus late linearization, indicating a thawing or respectively, increasing dark energy. This is further confirmed by mock data experiments. Accordingly, it is unlikely that the DESI pipeline is immune to the same contradiction.

Conclusions. Our results show rather than thawing, claimed by DESI, dark energy may in fact be increasing upon preserving the underlying symmetry. Further confirmation is expected from *Euclid*.

Key words. Cosmology — Dark energy — Cosmological constant — Expanding universe— Cosmological parameters — Deceleration parameter

1. Introduction

The observation of accelerated expansion of our Universe is a revolutionary discovery (Riess et al. 1998; Perlmutter et al. 1998, 1999). Since this discovery the concept of dark energy is at the frontier of modern cosmology. Although the existence of dark energy is confirmed, its origin and nature is still a mystery.

The common cosmological framework Λ CDM supports the idea of a constant dark energy, further substantiated by *Planck* CMB data (Planck Collaboration et al. 2020). The significance hereof cannot be overstated, in particular for the Λ CDM prediction of fluctuations in the *Cosmic Microwave Background* (CMB) containing the seeds for galaxy formation, imprinted in the *Baryon Acoustic Oscillations* (BAO) of the *Large Scale Structure* (LSS). However, there are emerging challenges to the assumed constant Λ in Λ CDM including but not limited to the significant tension in the Hubble constant H_0 , seen in the Local Distance Ladder (LDL) versus CMB analysis. H_0 -tension is the $> 5\sigma$ discrepancy between the H_0 values derived from the *Planck*- Λ CDM and that of LDL based on Parallax and Cepheids. These two limits of observation estimate $H_0 \simeq 67.36 \pm 0.54$ km s $^{-1}$ Mpc $^{-1}$ and, respectively, $H_0 \simeq 73.04 \pm 1.04$ km s $^{-1}$ Mpc $^{-1}$ (Planck Collaboration et al. 2020, Riess et al. 2022).

H_0 -tension has prompted considerable attention to studies and observations of possible varying dark energy in cosmological models beyond Λ CDM, most recently so by the DESI

(Adame et al. 2025). A common, but not exclusive, approach to study dynamical dark energy is $w(a)$ CDM framework, where $w(a) = PDE/\rho_{DE}$ stands for a general equation of state for dark energy as a function of Friedmann scale factor $a = 1/(z + 1)$, equivalently cosmological redshift z . The implementation hereof is frequently done by a linearization (Chevallier & Polarski 2001; Linder 2003)

$$w(a) = w_0 + (1 - a)w_a, \quad (1)$$

parameterized by the constants w_0 and w_a , as coefficients in the projection of a Taylor series of $w(a)$ to a polynomial of degree one, applied in the CPL formalism (Chevallier & Polarski 2001; Linder 2003). Based on CPL, DESI reports results for various cosmological parameters from their second data release (DR2) (DESI Collaboration et al. 2025b). A key claim by DESI is evidence for a thawing dark energy based on $-1 < w_0 < 0$ and $w_a < -1$ (DESI Collaboration et al. 2025b). In what follows, we shall use “thawing” when the location of w_0w_a -estimate is in the fourth quadrant of the w_0w_a -plane, centered about $(-1, 0)$. This is surprising as it is at odds with other studies specifically those involving LDL, let alone Λ CDM. Moreover, linearization is prone to systematic errors due to potential non-commutativities in the generally nonlinear data analysis pipelines, involving fits and linearization applied at different steps. In fact, the reliability of $w(a)$ parametrizations quite generally including CPL formalism has been questioned increasingly for over two decades (e.g. Huterer & Starkman (2003);

* Corresponding author

Ma & Zhang (2011); Feng et al. (2012); Pantazis et al. (2016); Ó Colgáin et al. (2021); Nesseris et al. (2025); Lee (2025)), but without addressing the underlying origin, which we will elucidate in the analysis presented below.

The DESI survey is produced by six independent observatories each looking at galaxies over a specific redshift range covering $z = 0.1$ to $z \approx 4$ (DESI Collaboration et al. 2025a). Although, DESI can not directly measure the Hubble constant H_0 , it nevertheless introduces novel constraints on it based on $\Omega_{m,0}$ estimation. Analyzing the data from galaxies, their main objective is to properly measure BAO in the LSS. Doing so accurately requires detailed considerations of spectral distortions due to nonlinear evolution and inhomogeneities in the low redshift distribution of galaxies.

Nevertheless, based on the *Planck*- Λ CDM analysis of the CMB there is a tight correlation between $\Omega_{m,0}$ and H_0 according to the BAO constraint

$$c_M = \Omega_{m,0} h^2, \quad (2)$$

giving $c_M^{\text{planck}} = 0.1424 \pm 0.00087$ where $h = H_0/100$ (Planck Collaboration et al. 2020).

Given the redshift range of DESI analysis ($0.1 < z \lesssim 2.3$), its results are expected to be consistent with the LDL (Lodha et al. 2025, Adame et al. 2025). Including the required considerations about spectral distortions, the final c_M values reported by DESI for different background cosmologies is consistent to within 5% of that of *Planck*- Λ CDM (DESI Collaboration et al. 2025b).

DESI adapts the linearized form (1) for a potentially varying dark energy. A key result is the above-mentioned thawing dark energy associated with $q_0 \sim -0.5$ consistent with that of Λ CDM, which is surprisingly in contradiction with other LDL analysis. Notably, we mention an appreciable discrepancy based on the estimate of the deceleration parameter $q_0^{\text{LDL}} = -1.08 \pm 0.29$ (Camarena & Marra 2020; De Simone et al. 2025).

Motivated by these discrepancies, in this work we focus on the *implementation* of linearization (1) in otherwise inherently nonlinear parameter estimation. We consider the potential for systematic errors in linearization that may arise from its application *early* or *late* in the pipeline, further details below. We demonstrate that in such linearization applied to $w(a)$ associated with (2), late linearization respects an underlying symmetry pertinent to the problem at hand while early linearization violates the same. In fact, the same applies to similar approximations.

To show the potential relevance to DESI, we demonstrate resulting systematics by applying it to the LDL using Farooq data (Farooq et al. 2017). The Farooq data is a compilation of Hubble parameter values within the Local Universe ($0.07 < z < 1.95$). It covers the LDL and is consistent with SHOES (Riess et al. 2022) in its estimates, in particular, of H_0 and q_0 . As a minimal data set, it is hereby ideally suited to demonstrate the above-mentioned symmetry violation and non-commutativity between $w_0 w_a$ CDM and a posteriori linearization of $w(a)$ CDM. However, our results persist regardless of choice of data.

We first discuss the $w(a)$ CDM cosmological model and its inherent symmetry together with its linearization from a first order Taylor series in §2. The core is presented in §3 with the data analysis implementation comprising data preparation, linearization and cosmological parameters estimation by application of Monte Carlo (MC) to the above-mentioned Farooq data as test data set. We interpret our results and its significance to DESI in §4. We conclude our findings for dynamical dark energy in §5.

2. Equation of state of dark energy

Λ CDM is the most common cosmological model in describing the evolution of the cosmos and assumes a constant dark energy Λ with $p_\Lambda/\rho_\Lambda = -1$. Though having a good fit to the *Planck*-CMB, it fails in accounting for galaxy formation at cosmic dawn and lower redshifts giving rise to many challenges (§1) (Bull et al. 2016; Perivolaropoulos & Skara 2022; Efstathiou 2025; Glazebrook et al. 2024; van Putten 2024).

A robust criterion derived from Λ CDM parameter estimation originates from the BAO (2) - the dimension-full energy density of baryonic and dark matter ρ_m - estimated by *Planck*- Λ CDM analysis of the CMB data (Planck Collaboration et al. 2020). Accordingly, Λ CDM based CMB analysis show $\Omega_{m,0} = 0.3135 \pm 0.0073$, and therefore $H_0 \simeq 67.36 \pm 0.54 \text{ km s}^{-1} \text{ Mpc}^{-1}$ (Planck Collaboration et al. 2020). These results are associated with a notably nice fit of the model to the CMB power spectrum except for low l , the consequences of which point to a need for further considerations beyond Λ CDM.

Many of the proposed models explore the potential of a dynamical dark energy (van Putten 2017; Avsajanishvili et al. 2024; Di Valentino et al. 2025). In a three flat universe when radiation can be neglected a general formulation is (See Appendix A for details of the following calculation)

$$H(a)^2 = H_0^2 \left[\Omega_{m,0} a^{-3} + (1 - \Omega_{m,0}) \hat{\rho}_{DE} \right], \quad (3)$$

where $\hat{\rho}_{DE} = A_0^{-1} A(a)$, $A(a) = H^2(a) - C_M a^{-3}$, $A_0 = (H_0^2 - C_M)$ and $C_M = \Omega_{m,0} H_0^2$ analogous to (2). In $w(a)$ CDM, $w(a)$ is defined by the expression $\hat{\rho}_{DE} \equiv \exp(f_{DE})$, based on the continuity equation for dark energy when $p_{DE} = w(a) \rho_{DE}$, giving

$$f_{DE} = -3 \int_a^1 \frac{1 + w(a')}{a'} da'. \quad (4)$$

An explicit expression for $w(a)$ derives accordingly from

$$w(a) = -1 - \frac{1}{3} \frac{d \ln \hat{\rho}_{DE}}{d \ln a} = -1 - \frac{1}{3} \frac{d \ln A(a)}{d \ln a} \quad (5)$$

independent of the normalization constant A_0 , dropping out by differentiation. In departure from Λ CDM, (2) may be subject to changes constraining model parameters. Consequently, we find $w(a)$ satisfies the invariance (Appendix A)

$$dw(a) \propto dc_M, \quad (6)$$

showing no dependencies on $\Omega_{m,0}$ or H_0 alone. This introduces an underlying symmetry. According to which

1. $w(a)$ is invariant with respect to *constraint-satisfying variations* in $\Omega_{m,0}$, preserving a constant c_M in (2);
2. $w(a)$ is not invariant with respect to *constraint-violating variations* in $\Omega_{m,0}$ in departures of the constraint (2).

The invariance of $w(a)$ in the first case presents a symmetry in $w(a)$ with respect to constrained variations in $\Omega_{m,0}$ in confrontation with data. As a physical property in cosmological evolution, this symmetry is to be respected in potential approximations to $w(a)$.

A common approximation to $w(a)$ CDM above, also applied by DESI, is $w_0 w_a$ CDM defined by using the relation (1) as an a priori linearization to the underlying $w(a)$. This is commonly

referred to as CPL. In this approximation, however, A_0 fails to drop out, taking (5) into

$$-(1 + w_0 + w_a) \ln a + w_a(1 - a) = \frac{1}{3} \ln (A(a)/A_0). \quad (7)$$

Here, the invariance (6) is now lost by explicit exposure to H_0^2 in A_0 . Thus, even in constraint-satisfying variations of $\Omega_{m,0}$, early linearization retains a finite sensitivity to $\Omega_{m,0}$ in departure of the exact symmetry (6) by the associated variations in H_0^2 . This introduces a potentially systematic error in the pipeline with significant observational consequences, regardless of the choice of data set (Appendices A and C).

In what follows, we focus on this potential for systematic uncertainties implied by the above-mentioned symmetry violation as a result of this linearization (1) through (7). We elaborate on this through (7) versus (5), pertaining to linearization (or similarly other approximations) *a priori* and, respectively, *a posteriori*. We next set out to demonstrate this in the LDL (see Appendix B for the test data).

3. Early and late implementation of linearization

Our starting point is $w(a)$ in (5) in analysis of data $H(a)$, with H_0 and $\Omega_{m,0}$ as free parameters, that may be anchored in the BAO constraint (2). Similar to DESI, we assume a three-flat universe as in (3) with $\Omega_k = 0$. To remain unbiased, we include constraint-satisfying variations in our control parameter $\Omega_{m,0} \in [0.22, 0.36]$, satisfying the c_M in (2) unless otherwise is specified. This is a sufficiently wide interval to cover all the conventional estimates of $\Omega_{m,0}$ along with, $H_0 \in [60, 80] \text{ km s}^{-1} \text{ Mpc}^{-1}$. For completeness, we also include sensitivity analyses to constraint-violating variations in $\Omega_{m,0}$.

As elucidated in Fig.B.1 we henceforth consider the following two distinct implementations

- I. Late linearization:** Extracting the samples $w(a_i)$ from (5) matching the data first, followed by the linear fit (1) for a w_0w_a -estimate (Fig. B.2; upper panels);
- II. Early linearization:** Extracting a w_0w_a -estimate directly from a fit of (7) to the data (Fig. B.2; lower panels).

In I the symmetry (6) is naturally satisfied, whereas in II it is invariably violated. Moreover, as shown in Fig. B.1, I and II are applying two different cost functions in finding (w_0, w_a) -estimates. As mentioned above, the results will be distinct due to a systematic error in the second and inherently different statistics.

4. Interpretation of Results

Prompted by inconsistencies in DESI results for dynamical dark energy with the LDL and Λ CDM, we consider (1) in the two distinct approaches I and II, defined in §3 here elucidated using the Farooq data of the LDL covering a similar redshift range as DESI, following the process in Appendix B. In our demonstration, the $\Omega_{m,0}$ of DESI produces two radically different results for (w_0, w_a) in late versus early linearization (Fig. 1, Table B.2). Crucially, preserving the fully nonlinear expression (5) together with late application of (1), (w_0, w_a) is identified to be in the second quadrant of w_0w_a -plane, *antipodal* to DESI's location in the fourth quadrant (Fig. 1) - here reproduced in the application of early linearization (7). The difference between the two results is evident by opposite slopes and different y-intercepts for (1) shown in Fig. B.3.

Notably, this result persists in early and late linearizations of mock $H(a)$ data produced using Λ CDM and CPL (Appendix C). For a given injected $\Omega_{m,0}$ and H_0 , Fig. C.1 shows that w_0w_a -estimates from late linearization are consistent with injections, robust against uncertainties in $\Omega_{m,0}$ as per (5). In aiming to constrain physical properties of dark energy, this robustness fulfills the requirement of specificity: insensitivity to other parameters, here the aforementioned constrained variations in matter density $\Omega_{m,0}$. Early linearization, in the same experiment, results in inconsistencies in w_0w_a -estimates whenever $\Omega_{m,0}$ is in departure of its underlying true value.

Table B.2 also lists results for $\Omega_{m,0} = 0.265$ with $H_0 = 73.30 \text{ km s}^{-1} \text{ Mpc}^{-1}$ consistent with LDL, for the two cases I and II discussed in §3. As expected from the inherent symmetry discussed in §2 for late linearization, our result on the quadrant containing (w_0, w_a) is robust with respect to constraint-satisfying variations in $\Omega_{m,0}$. See further Appendix D which includes also constraint-violating variations of $\Omega_{m,0}$. Fig. D.1 shows this in the persistence of the inconsistency between early and late linearizations. Based on this demonstration, we attribute the inconsistencies between DESI results and the LDL to the same, where early linearization insufficiently accounts for the underlying symmetries and nonlinearities in these parameter estimations. This is a serious systematic error in data analysis pipelines using CPL on stratified data more generally, including DESI.

Notably, the results on (w_0, q_0) from late linearization is in agreement with q_0 and w_0 , independently derived from the data through the Taylor series $H(z) = H_0(1 + (1 + q_0)z + \dots)$. Our results for late linearization are entirely consistent with the LDL, in particular in estimates of $(H_0, \Omega_{m,0}, w_0, w_a)$. Three of these four parameters are independent based on (2), and (w_0, w_a) is representative for the deceleration parameter. According to the late linearization of $w(a)CDM$, $q_0 = (3\Omega_{DE,0}w_0 + 1)/2$ (see (B.1)), we find $q_0 \simeq -1.3$ by the peak value in Fig. B.2, consistent with earlier estimates of q_0 in the LDL (van Putten 2017; Camarena & Marra 2020; De Simone et al. 2025).

Our estimate of (w_0, w_a) carries a discrepancy of 2σ and 1.6σ with respect to the DESI estimates. Additionally, applying (2) to $H_0 = 73.04 \text{ km s}^{-1} \text{ Mpc}^{-1}$ from LDL (Riess et al. 2022), $\Omega_{m,0} = 0.268$ is distinct from the DESI DR2 estimate by about 4.66σ . The combination of $\Omega_{m,0}$ and (w_0, w_a) estimates reveals a 4.94σ discrepancy between DESI and LDL. Fig. 1 shows this discrepancy in the location of the green island (late linearization, quadrant II) consistent with the LDL, and the red island (early linearization, quadrant IV) representative for DESI. Roughly equivalent, by the central values $q_{0,g} \simeq -1.3$ for green and $q_{0,r} \simeq -0.4$ for red, we have the inequalities $q_{0,g} < q_0^\Delta < q_{0,r}$. The first inequality is consistent with previous estimates of q_0 in the LDL showing a dark energy which is *increasing* in contrast to the second which implies the opposite.

Our analysis of early and late linearization (§3) is based on applying MC extended over a range of $\Omega_{m,0}, c_M$. In all cases, the red island turns out to be significantly unstable with respect to changes in $\Omega_{m,0}$ due to the symmetry breaking and inherent nonlinearities that are missed in *a priori* linearization (Appendix D). Notably, this discrepancy holds regardless of test data seen also when using mock data sets (Appendix C).

5. Conclusion

In this work we consider cosmological parameter estimation on a potentially dynamical dark energy expressed by the equation of state $w(a)$ (§2) addressing DESI, LDL and *Planck*- Λ CDM results. We do so pursuant to late and early linearization applied

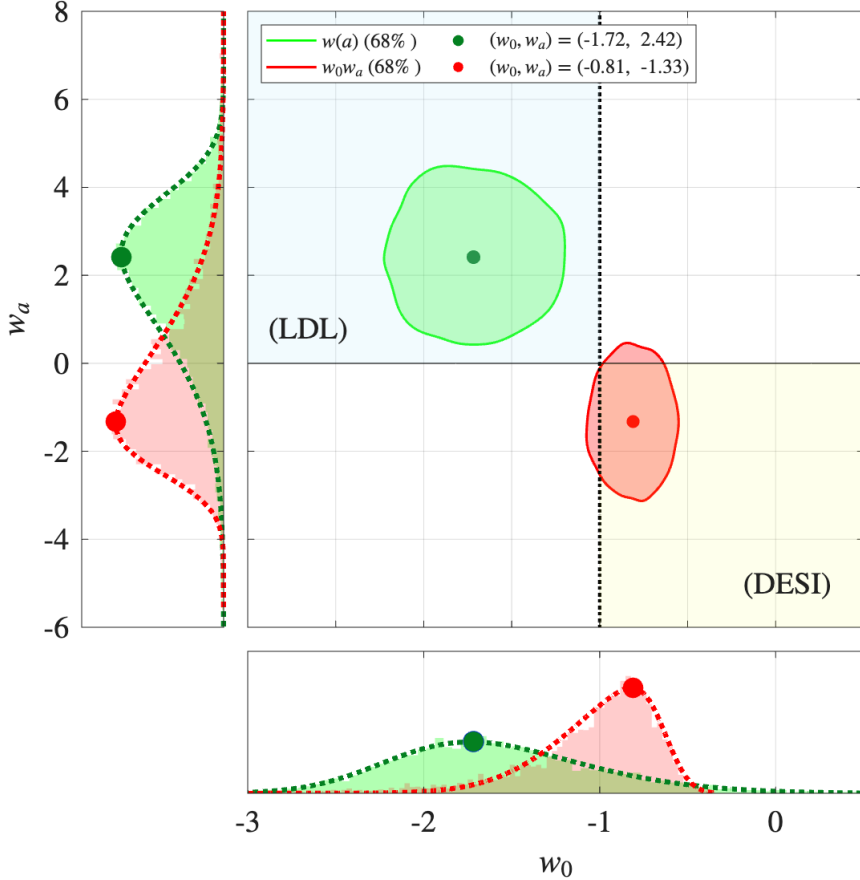


Fig. 1: Posterior plot for w_0 and w_a in the w_0w_a -plane in two distinct late and early (§B.2 and B.3) implementations of (1), respectively in green and red islands. This result strikingly shows a switch in quadrant from IV to II in fallback to the fully nonlinear expression (5) equivalent to the change in the slope and y -intercept of the linear approximations in Fig. B.3. According to (6), this is due to the violation of an underlying symmetry in red and non-commutativity between linearization and fit.

to tabulated data covering LDL (§B.1). The results of early and late linearization, *ceteris paribus*, are remarkably distinct due to the violation of symmetry (6) in the first, which is preserved in the second.

Detailed interpretation of our results derives from the w_0w_a -plane (Fig. 1). The green island in Fig. 1 shows late linearization following the nonlinear map (5) identifying (w_0, w_a) in quadrant II. This indicates an increasing dark energy consistent with the LDL, in agreement with q_0 and w_0 derived directly from $H(z)$ (Tables B.1 and B.2), including the results from Pantheon data over $z < 0.2$ (Camarena & Marra 2020), further confirmed by Pantheon and Pantheon+ data over the full range $z \lesssim 2.26$ (De Simone et al. 2025). Furthermore, late linearization turns out to be stable with respect to constraint-satisfying variations in $\Omega_{m,0}$ and regularly sensitive to variations in c_M (Appendix D, Fig. D.1) as expected from (5).

Conversely, the red island in Fig. 1 shows early linearization through (7) (applied also by DESI) identifying (w_0, w_a) in quadrant IV. This indicates a decreasing dark energy consistent with the DESI analysis (Table B.2). However, this is in 4.94σ disagreement, for instance, with regards to q_0 and w_0 derived directly from LDL.

Notably, the distinction between red and green islands and the quadrant containing the w_0w_a -estimates persists regardless of choice of data. This systematic discrepancy can only happen

because of the symmetry violation in early linearization. This indicates that upon applying an approximation, e.g. linearization, one should not be blind to the underlying intrinsic symmetries of the problem at hand. Accordingly, we conclude that early linearization is inapplicable.

The astrophysical consequences of our study indicating dark energy to be in the second quadrant of the w_0w_a -plane is that dark energy is increasing, in contradiction to DESI's claim.

Independent of DESI and LDL, the nature of dark energy may be decisively determined by the currently running *Euclid* mission (Euclid Mission (ESA) 2023). *Euclid* is in the process of measuring the BAO in a survey of about $O(10^9)$ galaxies up to a redshift of a few.

Acknowledgment

This work is supported by the National Research Foundation of Korea, under Grants No. NRF-RS-2024-00334550.

References

- Adame, A. G., Aguilar, J., Ahlen, S., et al. 2025, *J. Cosmol. Astropart. Phys.*, 2025, 021
- Aghaei Abchouyeh, M. & van Putten, M. H. P. M. 2021, *Physical Review D*, 104, 113502
- Alam, S., Ata, M., Bailey, S., et al. 2017, *Monthly Notices of the Royal Astronomical Society*, 470, 2617–2652

Avsajanishvili, O., Chitov, G. Y., Kahnashvili, T., Mandal, S., & Samushia, L. 2024, Universe, 10, 122

Blake, C., Brough, S., Colless, M., et al. 2012, Monthly Notices of the Royal Astronomical Society, 425, 405–414

Bull, P., Akrami, Y., Adamek, J., et al. 2016, Physics of the Dark Universe, 12, 56–99

Camarena, D. & Marra, V. 2020, Physical Review Research, 2

Chevallier, M. & Polarski, D. 2001, International Journal of Modern Physics D, 10, 213–223

De Simone, B., van Putten, M., Dainotti, M., & Lambiase, G. 2025, Journal of High Energy Astrophysics, 45, 290–298

Delubac, T., Bautista, J. E., Busca, N. G., et al. 2015, Astronomy & Astrophysics, 574, A59

DESI Collaboration, Abdul-Karim, M., Adame, A. G., et al. 2025a, arXiv e-prints, arXiv:2503.14745

DESI Collaboration, Abdul-Karim, M., Aguilar, J., Ahlen, S., & et. al. 2025b, arXiv e-prints, arXiv:2503.14738

Di Valentino, E., Said, J. L., Riess, A., et al. 2025, Physics of the Dark Universe, 49, 101965

Efstathiou, G. 2025, Philosophical Transactions of the Royal Society A: Mathematical, Physical and Engineering Sciences, 383

Euclid Mission (ESA). 2023, https://www.esa.int/Science_Exploration/Space_Science/Euclid, [Accessed 25-07-2025]

Farooq, O., Madiyar, F. R., Crandall, S., & Ratra, B. 2017, The Astrophysical Journal, 835, 26

Feng, C.-J., Shen, X.-Y., Li, P., & Li, X.-Z. 2012, Journal of Cosmology and Astroparticle Physics, 2012, 023–023

Font-Ribera, A., Kirkby, D., Busca, N., et al. 2014, Journal of Cosmology and Astroparticle Physics, 2014, 027–027

Glazebrook, K., Nanayakkara, T., Schreiber, C., et al. 2024, Nature, 628, 277–281

Huterer, D. & Starkman, G. 2003, Phys. Rev. Lett., 90, 031301

Lee, S. 2025, arXiv e-prints, arXiv:2506.18230

Linder, E. V. 2003, Physical Review Letters, 90

Lodha, K., Shafieloo, A., Calderon, R., et al. 2025, Physical Review D, 111

Ma, J.-Z. & Zhang, X. 2011, Physics Letters B, 699, 233–238

Moresco, M. 2015, Monthly Notices of the Royal Astronomical Society: Letters, 450, L16–L20

Moresco, M., Cimatti, A., Jimenez, R., et al. 2012, Journal of Cosmology and Astroparticle Physics, 2012, 006–006

Moresco, M., Pozzetti, L., Cimatti, A., et al. 2016, Journal of Cosmology and Astroparticle Physics, 2016, 014–014

Nesseris, S., Akrami, Y., & Starkman, G. D. 2025, arXiv e-prints, arXiv:2503.22529

Pantazis, G., Nesseris, S., & Perivolaropoulos, L. 2016, Physical Review D, 93

Perivolaropoulos, L. & Skara, F. 2022, New Astronomy Reviews, 95, 101659

Perlmutter, S., Aldering, G., Goldhaber, G., et al. 1999, The Astrophysical Journal, 517, 565–586

Perlmutter, S., Aldering, G., Valle, M. D., et al. 1998, Nature, 391, 51–54

Planck Collaboration, Aghanim, N., Akrami, Y., et al. 2020, A&A, 641, A6

Riess, A. G., Filippenko, A. V., Challis, P., et al. 1998, The Astronomical Journal, 116, 1009–1038

Riess, A. G., Yuan, W., Macri, L. M., et al. 2022, The Astrophysical Journal Letters, 934, L7

Simon, J., Verde, L., & Jimenez, R. 2005, Physical Review D, 71

Stern, D., Jimenez, R., Verde, L., Kamionkowski, M., & Stanford, S. A. 2010, Journal of Cosmology and Astroparticle Physics, 2010, 008–008

van Putten, M. H. P. M. 2017, The Astrophysical Journal, 848, 28

van Putten, M. H. P. M. 2017, Modern Physics Letters A, 32, 1730019

van Putten, M. H. P. M. 2024, Physics of the Dark Universe, 43, 101417

Zhang, C., Zhang, H., Yuan, S., et al. 2014, Research in Astronomy and Astrophysics, 14, 1221–1233

Ó Colgáin, E., Sheikh-Jabbari, M., & Yin, L. 2021, Physical Review D, 104

Appendix A: The underlying symmetry

In $w(a)$ CDM, the defining relation of the equation of state $w(a)$ for dark energy follows energy conservation and the continuity equation. In a three-flat universe at late times, this starts with the Hamiltonian energy constraint

$$\Omega_m + \Omega_{DE} = 1 \quad (\text{A.1})$$

on the dimensionless density of matter, $\Omega_m = \rho_m/\rho_c$, and dark energy, $\Omega_{DE} = \rho_{DE}/\rho_c$, normalized to closure density $\rho_c = 3H^2/8\pi G$ given the Hubble parameter $H \equiv H(a)$. Densities of cold baryonic and dark matter scale with a^{-3} , i.e., $\rho_m = \rho_{m,0}a^{-3}$ and $\Omega_{m,0} = \rho_{m,0}/\rho_c$, where $\rho_c = \rho_{c,0}(H/H_0)^2$ and H_0 is the Hubble constant. Normalizing ρ_{DE} to $\rho_{c,0}$, $\hat{\rho}_{DE} \equiv \rho_{DE}/\rho_{c,0} = \Omega_{DE}(H^2/H_0^2)$, (A.1) satisfies (3). Accordingly, we have

$$\hat{\rho}_{DE} = A_0^{-1}A(a), \quad (\text{A.2})$$

where $A(a) = [H(a)^2 - \Omega_{m,0}H_0^2a^{-3}]$ is normalized to the constant $A_0 = (1 - \Omega_{m,0})H_0^2$. In $w(a)$ CDM, $w(a)$ is defined by the expression $\hat{\rho}_{DE} \equiv \exp(f_{DE})$, where f_{DE} is defined by (4) based on the continuity equation for dark energy, taking (3) into $H^2(a) = H_0^2[\Omega_{m,0}a^{-3} + (1 - \Omega_{m,0})\exp(f_{DE})]$. Accordingly, we arrive at (5) *independent* of the normalization constant A_0 , which is dropped out by differentiation, where the right-hand side is determined by data, H_0 and $\Omega_{m,0}$.

In light of the power spectrum of the CMB, we next consider the BAO constraint (2) where c_M is a constant. In particular, $c_M = 0.1424 \pm 0.0008$ according to *Planck* Λ CDM analysis. Due to model-dependency in the numerical value of c_M , $w(a)$ estimation is commonly explored over different values, notably by varying the control parameter $\Omega_{m,0}$ (Fig. B.1). Given a cosmic chronometer data $(z_i, h(z_i))$ over $z_i > 0$, we have $A = H(a)^2 - C_M a^{-3}$ by (2), whereby (5) implies the identity

$$dw(a) \equiv \left(1 + \frac{C_M a^{-3}}{A}\right) \left(\frac{a^{-3}}{A}\right) dC_M \propto dc_M. \quad (\text{A.3})$$

Thus, $w(a)$ is invariant to variations $\delta c_M = h^2 \delta \Omega_{m,0} + \Omega_{m,0} \delta h^2 = 0$, leaving sensitivity only to constraint-violating variations $\delta c_M \neq 0$. Following Fig. B.1, the invariance of $w(a)$ to $\delta c_M = 0$ carries over to $w_0 w_a$ -estimates by late linearization based on χ^2 -fits in the $w(a)$ -plane.

In contrast with the exact analysis above, early linearization which is in terms of $w_0 w_a$ – a null-hypothesis – allowing integration of f_{DE} up front, arrives at the algebraic relation (7). As before, the right-hand side is determined by data $(a_i, h(a_i))$ ($0 < a_i < 1$), the control parameter $\Omega_{m,0}$ and H_0 . The approximation (7) allows for $w_0 w_a$ -estimates from χ^2 -fits to (7) in the plane of $(a, h(a))$ data (Fig. 2), testing the null-hypothesis of a linear $w(a)$ relation with or without imposing the constraint (2). Notably, however, (7) carries explicit dependence on A_0 , otherwise absent in (5). In particular, (7) depends on a choice of H_0 by $A_0 = H_0^2 - C_M$, whereby *the symmetry (6) is fundamentally lost in early linearization*.

Summarizing, sensitivity in $w_0 w_a$ -estimates satisfy the following:

1. Late linearization preserves invariance to $\delta c_M = 0$;
2. Earlier linearization fails to satisfy invariance to $\delta c_M = 0$, leaving explicit sensitivity to H_0 , hence $\Omega_{m,0}$.

This presents a fundamental distinction between $w_0 w_a$ -estimation by late and early linearization, giving rise in particular to anomalous sensitivity to $\delta \Omega_{m,0}$ along the BAO constraint (2), regardless of the specific value of c_M . This distinction has important observational consequences for analysis of dark energy in the late time Universe.

Appendix B: $H(z)$ data and data processing

As mentioned in §2, our results on discrepancies between late and early linearization persist regardless of data in use (even mock data can be used for this purpose as presented in Appendix C). Here, we choose the Farooq data (Farooq et al. 2017) for simplicity and considering that it covers similar redshift range as in DESI. The Farooq data are cosmic chronometer data listed in Table B.1. Given that the data are provided with their associated redshift, we use the relation $a = 1/(1+z)$ to move to the redshift space for our analysis.

Table B.1: Hubble parameter versus redshift data

z_i	$H(z)$ (km s $^{-1}$ Mpc $^{-1}$)	σ_H (km s $^{-1}$ Mpc $^{-1}$)	Reference
0.070	69	19.6	5
0.090	69	12	1
0.120	68.6	26.2	5
0.170	83	8	1
0.179	75	4	3
0.199	75	5	3
0.200	72.9	29.6	5
0.270	77	14	1
0.280	88.8	36.6	5
0.352	83	14	3
0.380	81.5	1.9	10
0.3802	83	13.5	9
0.400	95	17	1
0.4004	77	10.2	9
0.4247	87.1	11.2	9
0.440*	82.6	7.8	4
0.4497	92.8	12.9	9
0.4783	80.9	9	9
0.480	97	62	2
0.510*	90.4	1.9	10
0.593	104	13	3
0.600*	87.9	6.1	4
0.610*	97.3	2.1	10
0.680	92	8	3
0.730*	97.3	7	4
0.781	105	12	3
0.875	125	17	3
0.880	90	40	2
0.900	117	23	1
1.037	154	20	3
1.300	168	17	1
1.363	160	33.6	8
1.430	177	18	1
1.530	140	14	1
1.750	202	40	1
1.965	186.5	50.4	8
2.340*	222	7	7
2.360*	226	8	6

-Reprinted from (Farooq et al. 2017).

* These data points have underlying Λ CDM dependencies and are excluded from our analysis.

(1) Simon et al. (2005); (2) Stern et al. (2010); (3) Moresco et al. (2012); (4) Blake et al. (2012); (5) Zhang et al. (2014); (6) Font-Ribera et al. (2014); (7) Delubac et al. (2015); (8) Moresco (2015); (9) Moresco et al. (2016); (3) Alam et al. (2017).

These data go through the processes shown in Fig. B.1 for late (I) versus early (II) linearization to realize the effect of the violated symmetry and ignored nonlinearities. Numerically one of the differences between I and II is in the implementation of χ^2 for the linearization (1). In I, χ^2 is implemented in $w(z)$ -space according to δ_L in Fig. B.1, where δ_L is the scatter in $w(z)$ -space. In

II, on the other hand, χ^2 is implemented in $H(z)$ -space according to the scatter δ_E .

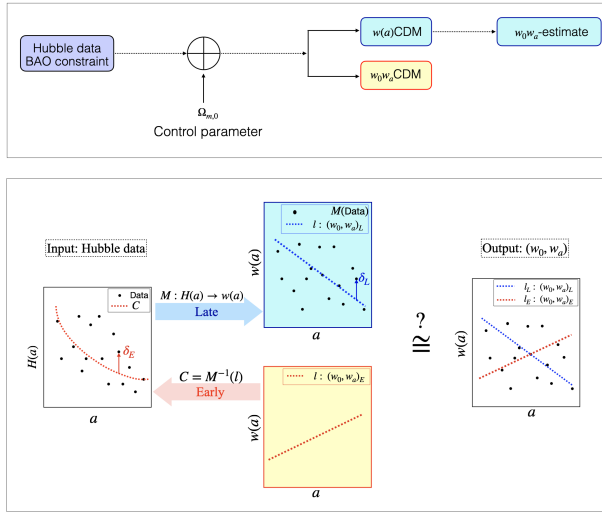


Fig. B.1: (Upper panel.) Flowchart of the late (I) and early (II) implementation of linearization l according to (1) in the $w(a)$ CDM formalism, starting from the Farooq data of the LDL, and the *Planck*-BAO constraint supplemented with the control parameter $\Omega_{m,0}$ (§3). As shown in §4, the results of these two implementations appear in different quadrants of w_0w_a -plane. (Lower panel.) Schematic of the implementations of early and late linearization in estimating w_0 and w_a where M refers to (5): early linearization minimizes χ^2 in $H(z)$ -space according to the scatter δ_E , while late linearization minimizes χ^2 in $w(z)$ -space according to the scatter δ_L following the nonlinear map (5). The question is to what extent the output of these two implementations agree *ceteris paribus*, including their sensitivities to $\Omega_{m,0}$.

B.1. Data preparation and methods

Starting from Table B.1, we first perform a smoothing process using a polynomial fit to $H(z_i)$ with weights $1/\sigma_i^2$ (van Putten 2017; Aghaei Abchouyeh & van Putten 2021). As in previous work, we find satisfactory fits for a cubic and quartic polynomial, the latter with slightly higher residuals.

To peruse our analysis on w_0w_a -estimates including uncertainties, we perform MC process on N trials defined by randomly chosen Hubble parameter data within the interval $H(z_i) \pm 1\sigma_i$ in the Farooq data, where we use $N = 5000$. Each trial is smoothed by the aforementioned cubic fit. At this level the PDF of H_0 and as a result also q_0 can be derived, here defined by the first two terms in the Taylor series expansion of $H(z)$.

The resulting estimates $H_0 = 75.88^{+4.79}_{-4.59} \text{ km s}^{-1} \text{ Mpc}^{-1}$ and $q_0 = -1.39^{+0.33}_{-0.28}$ are consistent with LDL. Notably, our $q_0 = -1.39^{+0.33}_{-0.28}$ estimate is entirely consistent with $q_0 = -1.08 \pm 0.29$ independently derived from the Pantheon sample of type Ia Supernovae (Camarena & Marra 2020; De Simone et al. 2025), whose combined estimate shows a 3σ departure from q_0^Λ of the *Planck*- Λ CDM estimate, $q_0^\Lambda \simeq -0.527$. Furthermore, for a three flat universe where radiation can be neglected

$$w(z) = \frac{2q(z) - 1}{3\Omega_{DE}(z)}, \quad (\text{B.1})$$

giving $w_0 = -1.8^{+0.32}_{-0.27}$ which is less than that of Λ CDM (see further De Simone et al. (2025)). Largely model-independent, these values of q_0 and w_0 serve as reference points in the two implementations (I) and (II) ensuring that the two implementations do not create significant deviations from what data offers as starting point (§4).

B.2. Late linearization

Applying the MC process with $N = O(10^3)$ mentioned in §B.1, we realize implementation (I) - late linearization - producing $w(z_i)$ values over all z_i of Table B.1 using the invertible map (5). This transfers the calculation from $H(z)$ -space to $w(z)$ -space (Fig. B.1) with no loss of information. In this process H_0 derives from (2) based on a choice of the control parameter $\Omega_{m,0}$. For H_0 from the LDL this would correspond to $\Omega_{m,0} \simeq 0.265$, included in our analysis covering a broad range of $\Omega_{m,0}$ values.

We next extract w_0w_a -estimates from the $w(z_i)$, through a linear fit to $w(z_i)$, using (1). The resulting PDFs are shown in Fig. B.2. According to §2, late linearization produces (w_0, w_a) -estimates that are invariant of variations in $\Omega_{m,0}$ when the constraint (2) is satisfied.

We therefore observe $w_0 < -1$, consistent with results from (B.1), and $w_a > 0$. This, in its own right, shows late linearization to be loyal to the data in use due to consistency with w_0 derived in §B.1.

B.3. Early linearization

Next, we turn to the second implementation II using (7), that is an *a priori* inclusion of linearization (1). This is done in $H(z)$ -space defined in (7). Fig. B.2 shows the resulting PDFs of w_0w_a -estimates for a choice of $\Omega_{m,0}$. Strikingly, we now observe $-1 < w_0 < 0$ and $w_a < 0$, in contradiction to that of the initial data, though consistent with DESI's results. This originates from the broken symmetry in (5), hence the non-commutativity between w_0w_a CDM and a posteriori linearization of $w(a)$ CDM, also the change in the cost function.

Appendix C: Early and late linearizations on mock data

Applying early and late linearization on the Farooq data for w_0w_a -estimate shows the results to be in two antipodal quadrants, IV and II. To confirm that this result is not biased by the data in use we applied the same methods to series of mock data reproduced by functions for $w(a)$, here CPL (see (7)) and Λ CDM.

To produce mock data we choose $\Omega_{m,0} = 0.27$ that satisfies (2). For Λ CDM, $H(a)$ satisfies

$$H(a) = H_0 \sqrt{1 + \Omega_{m,0}(a^{-3} - 1)}, \quad (\text{C.1})$$

where $w_0 = -1$ and $w_a = 0$, by definition.

For CPL we set $w_0 = -1.5$ and $w_a = 2$ in (7), without loss of generality. Consequently we have two set of mock $H(a)$ data to go through early and late linearizations.

Using (1), (5) and (7), we then estimate w_0 and w_a using early and late linearizations separately for Λ CDM and CPL. The results confirm that of the Farooq data as shown in Fig. C.1: Early and late linearization do not give consistent results for w_0w_a -estimate, and early linearization is significantly sensitive to the control parameter $\Omega_{m,0}$ as expected from Appendix A.

Table B.2: (w_0, w_a) results using Farooq data (Farooq et al. 2017) in early versus late linearization (§3) compared with those of Planck ΛCDM and DESI.

Parameter	Planck ΛCDM	Farooq et.al. data		DESI DR2
		Late linearization	Early linearization	
$\Omega_{m,0}$	$0.3153^{+0.0073}_{-0.0073}$	0.265	0.352	$0.352^{+0.041}_{-0.018}$
H_0 (km s $^{-1}$ Mpc $^{-1}$)	67.36	73.30	63.60	63.60
w_0	-1	$-1.72^{+0.39}_{-0.3}$	$-1.68^{+0.36}_{-0.34}$	$-0.81^{+0.1}_{-0.24}$
w_a	0	$2.42^{+0.8}_{-1.72}$	$2.49^{+0.81}_{-1.76}$	$-1.33^{+1.22}_{-1.06}$
				$-2.72^{+1.31}_{-1.11}$
				< -1.34

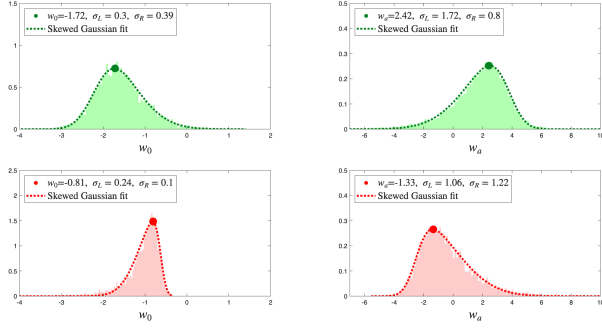


Fig. B.2: (Upper panels.) PDFs of w_0 and w_a derived from our MC in late linearization (§B.2) which are invariant under the choice of $\Omega_{m,0}$ satisfying the constraint (2)(§2). (Lower panels.) PDFs of w_0 and w_a derived from our MC in early linearization (§B.3) which is not invariant under the choice of $\Omega_{m,0}$ satisfying the constraint (2). In these examples, $\Omega_{m,0} = 0.265$ is associated with $H_0 = 73.3$ km s $^{-1}$ Mpc $^{-1}$ by (2). The peak of the skewed Gaussian fit shows the nominal values of w_0 and w_a . Paradoxically, early linearization (lower panels) gives rise to nonlinear propagation of uncertainties seen in the non-Gaussian PDFs of (w_0, w_a) , more so than in late linearization (upper panels). Although the peak value may be slightly different, the discrepancy between the two implementations persist for the entire ensemble covering the whole range $\Omega_{m,0} \in [0.22, 0.36]$.

It is evident from Fig. C.1 that $w_0 w_a$ -estimates from late linearization are consistent with injections, robust against uncertainties in $\Omega_{m,0}$ as per (5), in contrast to early linearization due to its parasitic sensitivity to the same.

Appendix D: Constraint-satisfying and constraint-violating variations in $\Omega_{m,0}$

Fig. 1 is the final result for the estimations of w_0 and w_a we derive from two different approaches for linearizing $w(a)$ (late and early §3). This result may be subject to sensitivities to the involved BAO constraint on c_M (2) as shown in (6). The parameter values used in Fig. 1 are consistent with LDL having $\Omega_{m,0} = 0.265$ and $H_0 = 73.30$ km s $^{-1}$ Mpc $^{-1}$. To illustrate the sensitivity of late and early linearization to these parameters we loosen the BAO constraint by 20% lower or higher than the Planck estimate. Here we also include our analysis for both $\Omega_{m,0} = 0.265$ of LDL and $\Omega_{m,0} = 0.352$ of DESI analysis.

Fig. D.1 shows the sensitivity to changes in c_M and $\Omega_{m,0}$. Noticeably an increase in c_M , shifts w_0 to lower values in both early (red) and late (green) linearization. On the other hand it increases w_a in the green island, while decreases the same in the

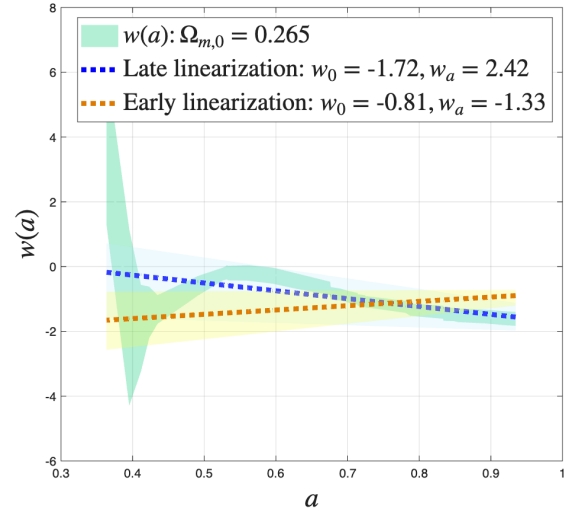


Fig. B.3: The evolution of $w(a)$ in (5) and its linearization (1) in late and early implementations following Fig. B.1. The green shaded region shows $w(z_i)$ following the application of the map (5) on Farooq data including an MC process. The blue dotted line is the result from late linearization (1) on $w(z_i)$ (§B.2), clearly showing a negative slope indicative for $w_a > 0$. The red dotted line, on the other hand, is the result of early linearization by application of (7) on the Farooq data showing a positive slope. The distinct slopes of the two demonstrate that the implementation of the linearization (1) is non-commutative with the fitting process, answering the question raised in Fig. B.1.

red island. These changes, although in opposite directions, are of the same order of magnitude.

A change in $\Omega_{m,0}$ while keeping c_M constant has a different effect. As expected from (6), the green remains unchanged, shown in rows of Fig. D.1. In contrast, the red has noticeable sensitivity to this change taking the result to higher w_0 and lower w_a values. Following Fig. D.1, this can be summarized by, respectively

$$\begin{pmatrix} \frac{\partial w_0}{\partial \Omega_{m,0}} \\ \frac{\partial w_a}{\partial \Omega_{m,0}} \end{pmatrix}_g = \begin{pmatrix} -0.57 \\ -0.69 \end{pmatrix}, \quad \begin{pmatrix} \frac{\partial w_0}{\partial \Omega_{m,0}} \\ \frac{\partial w_a}{\partial \Omega_{m,0}} \end{pmatrix}_r = \begin{pmatrix} 7.93 \\ -14.83 \end{pmatrix}, \quad (\text{D.1})$$

where the results for green are indeed statistically consistent with zero. These sensitivities to constraint-satisfying variations in $\Omega_{m,0}$ are revealing: late linearization results remain stable, while early linearization appears dramatically unstable, expressed by

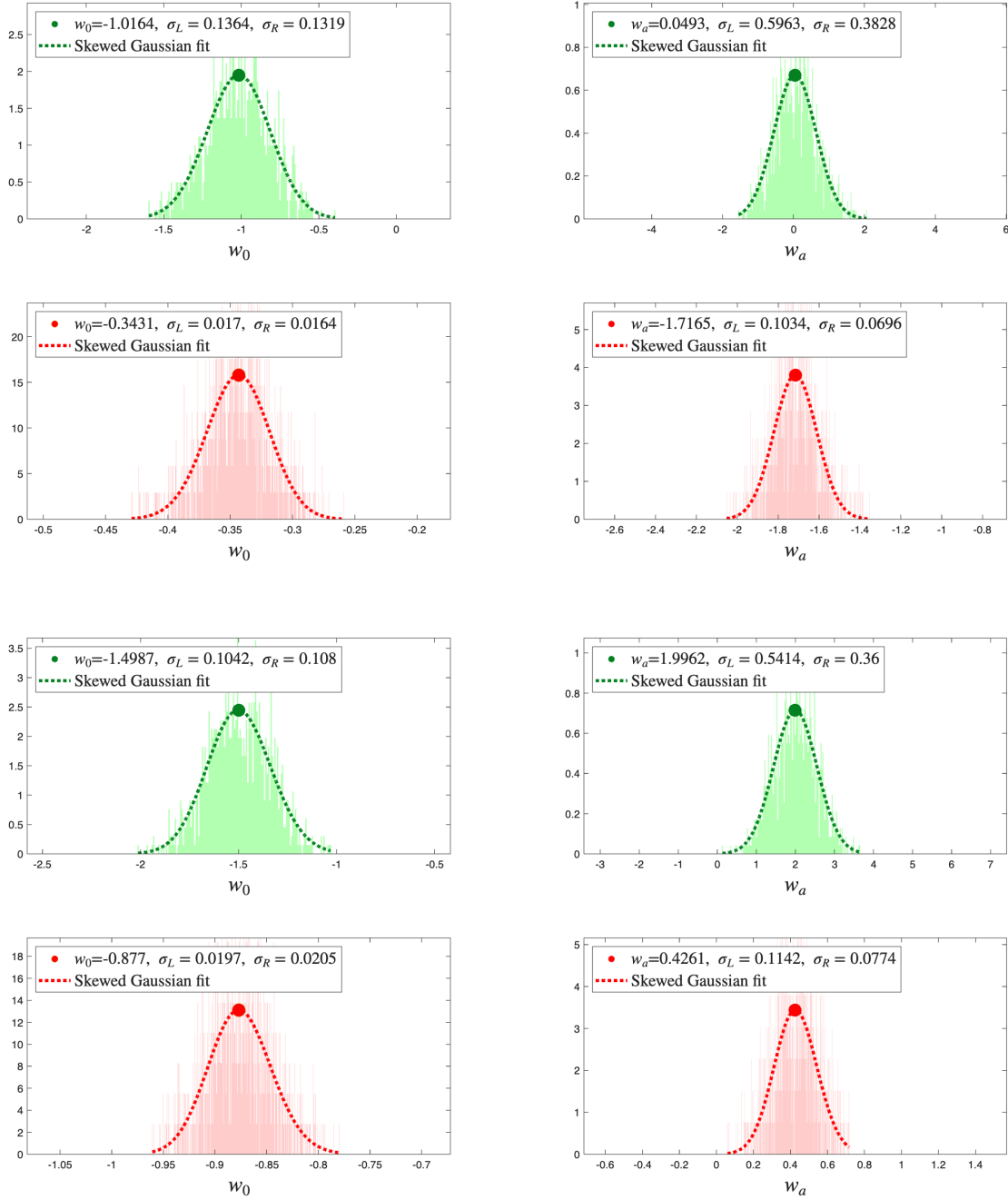


Fig. C.1: Results of early and late linearization in estimating w_0 and w_a . (Four upper panels). w_0w_a -estimate on Λ CDM mock data created using the injection $\Omega_{m,0_i} = 0.27$, carrying $w_0 = -1$ and $w_a = 0$. This figure is a snapshot of the results when the control parameter is $\Omega_{m,0} = 0.35$. While green (late linearization) gives consistent results with the underlying data regardless of $\Omega_{m,0}$, as per (5), red (early linearization), in contrast, exhibits parasitic sensitivity to the control parameter $\Omega_{m,0}$ (see also (D.1)), and is consistent with green only when $\Omega_{m,0} = \Omega_{m,0_i}$. (Four lower panels). The same using data produced by CPL where $w_0 = -1.5$ and $w_a = 2$. Clearly green gives results consistent with initial injections for w_0 and w_a , but it is absent for red.

$$\left| \frac{(\partial w_0 / \partial \Omega_{m,0})_r}{(\partial w_0 / \partial \Omega_{m,0})_g} \right| = 13.9 \quad \text{and} \quad \left| \frac{(\partial w_a / \partial \Omega_{m,0})_r}{(\partial w_a / \partial \Omega_{m,0})_g} \right| = 21.5. \quad (\text{D.2})$$

These anomalous ratios indicate that early linearization is inapplicable to this nonlinear problem.

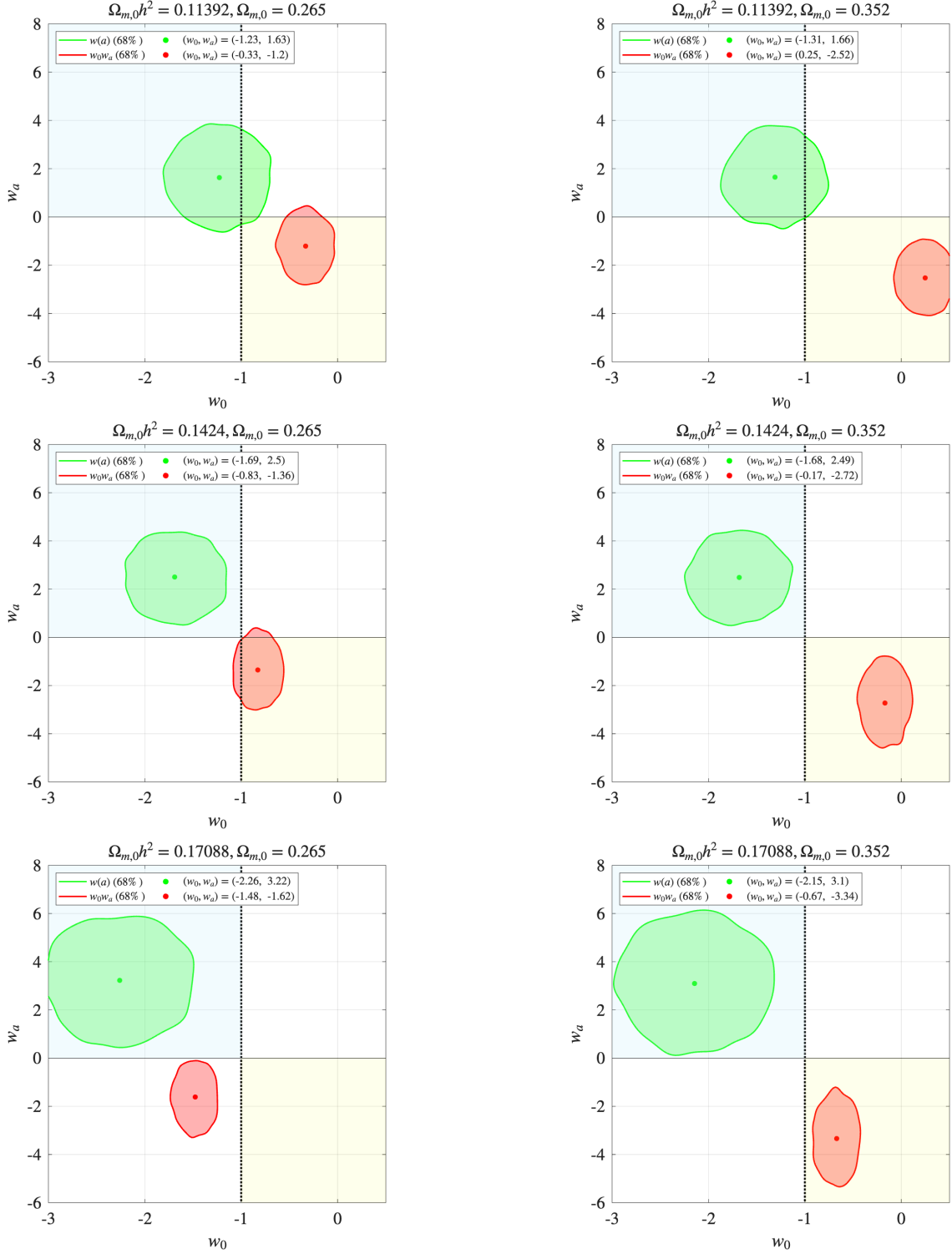


Fig. D.1: Sensitivity of our results in (w_0w_a) -plane to the choice of $\Omega_{m,0}$ and c_M with green and red to be representative for late and early linearization, respectively. Rows show sensitivity to constraint-satisfying variations for two values of $\Omega_{m,0}$; columns show sensitivity to constraint-violating variations for three values of c_M . Increasing c_M and keeping $\Omega_{m,0}$ constant moves both green and red to lower w_0 and higher (similar) w_a . On the contrary, keeping c_M constant and increasing $\Omega_{m,0}$ does not affect the result for green, due to the underlying symmetry in (5) that is respected in late linearization, but pushes the red island to south east, higher w_0 and lower w_a . These sensitivities are quantified in D.1 and D.2.